

# PCCP

Physical Chemistry Chemical Physics

Accepted Manuscript

This article can be cited before page numbers have been issued, to do this please use: D. Malpicci, E. Lucenti, L. Zecchinello, D. Marinotto, E. Cariati and A. Forni, *Phys. Chem. Chem. Phys.*, 2026, DOI: 10.1039/D5CP03691G.



This is an Accepted Manuscript, which has been through the Royal Society of Chemistry peer review process and has been accepted for publication.

Accepted Manuscripts are published online shortly after acceptance, before technical editing, formatting and proof reading. Using this free service, authors can make their results available to the community, in citable form, before we publish the edited article. We will replace this Accepted Manuscript with the edited and formatted Advance Article as soon as it is available.

You can find more information about Accepted Manuscripts in the [Information for Authors](#).

Please note that technical editing may introduce minor changes to the text and/or graphics, which may alter content. The journal's standard [Terms & Conditions](#) and the [Ethical guidelines](#) still apply. In no event shall the Royal Society of Chemistry be held responsible for any errors or omissions in this Accepted Manuscript or any consequences arising from the use of any information it contains.

## ARTICLE

Intra- and Intermolecular H-Bonds and  $\pi$ - $\pi$  Stacking Driven Organization of a Triazine-Based Room Temperature Phosphorescent Emitter<sup>†</sup>Daniele Malpicci,<sup>a,b</sup> Elena Lucenti,<sup>b</sup> Luca Zecchinello,<sup>a,b</sup> Daniele Marinotto,<sup>b</sup> Elena Cariati,<sup>\*a,b</sup> and Alessandra Forni<sup>\*b</sup>Received 00th January 20xx,  
Accepted 00th January 20xx

DOI: 10.1039/x0xx00000x

Excitation dependent, multiemissive single component organic materials are receiving evergrowing attention for various applications. In this regard, intermolecular interactions have revealed efficacious in positively affecting photoluminescent features. Here, the photophysical properties of **TT-2PyH<sup>+</sup>NO<sub>3</sub><sup>-</sup>** characterized by fluorescence and dual phosphorescence with ultralong contribution, are interpreted through DFT-TDDFT calculations and crystal structure analysis. The compound's locked molecular conformation through intramolecular hydrogen bond is at the basis of suppression of the low energy fluorescence displayed by its parent neutral derivative. On the other side,  $\pi$ - $\pi$  interactions are deemed responsible for the ultralong RTP features and the highly dense network of intermolecular hydrogen bonds provides a rigid molecular environment which efficiently restrict the non-radiative deactivation channels of triplet excitons.

## Introduction

Organic single component materials characterized by rich emissive behavior, comprising molecular and possibly supramolecular excitation-dependent fluorescence and room temperature phosphorescence (RTP), are receiving increasing attention from the scientific community due to the advantages they offer in different fields (*e.g.* bioimaging,<sup>1-3</sup> anticounterfeiting,<sup>4-8</sup> displays<sup>9</sup>). In particular, the number of purely organic long-lived phosphors is rapidly growing thanks to the advancements in molecular design and supramolecular engineering aimed at promoting singlet-to-triplet intersystem crossing (ISC) and suppressing non-radiative decay from excited triplet states.<sup>10-14</sup>

Particularly important, in this context, are organic compounds displaying ultralong RTP, a persistent luminescence with emission lifetimes of over 100 ms. To achieve RTUP, a rigid molecular environment, able to reduce molecular motions and thus stabilize the triplet excitons from nonradiative decay, represents a necessary condition. To this aim, several types of intra- and intermolecular interactions, including hydrogen bonds, halogen bonds, ionic bonds, and  $\pi$ - $\pi$  interactions, have been exploited.<sup>15-23</sup> Notably, hydrogen bonding has been demonstrated particularly efficacious in rigidifying the

molecular conformations and decreasing non-radiative deactivation channels of triplet excitons, contributing to phosphorescence lifetimes and enhancing quantum yield.<sup>24-26</sup>

As a contribution to this important research field, we have recently developed a wide family of compounds based on triimidazo[1,2-*a*:1',2'-*c*:1'',2''-*e*][1,3,5]triazine or cyclic triimidazole (from hereafter **TT**), characterized by a rich photophysical behavior comprising multiple fluorescence and phosphorescence of molecular and supramolecular origins, anti-Kasha emissions and excitation dependent photoluminescence.<sup>27</sup> In **TT** prototype itself, the role of  $\pi$ - $\pi$  interactions in activating radiative deactivation channels (fluorescence and RTUP lasting up to 1 s) through distortion of the C<sub>3h</sub> symmetry has been highlighted. Moreover, for many **TTs**  $\pi$ - $\pi$  interactions were demonstrated relevant in affecting their photophysics and responsible for their mechanochromic features.

In this context, previous studies on 3-(pyridin-2-yl)triimidazotriazine (**TT-2Py**), the pyridine derivative with the pyridinic nitrogen atom in ortho position with respect to **TT**, revealed a multifaceted, excitation dependent emissive behaviour comprising dual fluorescence and multiple phosphorescences.<sup>28, 29</sup> The origin of each contribution was explained, through deep experimental and theoretical investigation, on the basis of its molecular and supramolecular features.<sup>28</sup> In particular, the role of the partial rotational freedom of the pyridine ring in the compound's photoluminescence was disclosed. In addition to its appealing emissive properties, this compound revealed to be highly efficient in the preparation of coordination complexes and coordination polymers (CPs),<sup>30-32</sup> thanks to the coordinating ability of pyridine and **TT** itself.<sup>33-35</sup> Among metal containing derivatives, particularly noteworthy in view of its

<sup>a</sup> Department of Chemistry, Università degli Studi di Milano, via Golgi 19, 20133 Milano (Italy). E-mail: [elena.cariati@unimi.it](mailto:elena.cariati@unimi.it)

<sup>b</sup> Institute of Chemical Sciences and Technologies "Giulio Natta" (SCITEC) of CNR, via Golgi 19, 20133 Milano, Italy. Email: [alessandra.forni@scitec.cnr.it](mailto:alessandra.forni@scitec.cnr.it)

<sup>†</sup> Dedicated to Professor Resnati, celebrating a career in fluorine and noncovalent chemistry on the occasion of his 70th birthday

Supplementary Information available: Photophysical Data, Computational Results, Crystallographic Data and NMR Spectra. See DOI: 10.1039/x0xx00000x



photoluminescence properties, is the emissive Cu(I)-based CP, displaying an intriguing and rare structural motif comprising a double-stranded (CuI)<sub>2</sub> stair and a single CuI zig-zag chain.<sup>30</sup> Here, after a brief recap of the structural and photophysical features of **TT-2Py**, we report on the synthesis, characterization and photophysical investigation of its protonated derivative, **TT-2PyH<sup>+</sup>**. Besides revealing interesting photophysical properties, including dual phosphorescence with ultralong contribution, this compound displays a locked molecular conformation through intramolecular hydrogen bond (HB), which is demonstrated to be responsible for the suppression of the low energy fluorescence of the parent neutral derivative, allowing to support previous interpretation of the photophysical behaviour.

## Results and discussion

According to previous studies, **TT-2Py** was isolated in three polymorphs depending on the recrystallization solvent.<sup>28</sup> All of them display, in their crystal structure,  $\pi$ - $\pi$  stacking interactions among **TT** moieties, characterized by slightly different intermolecular distances and slippage features. The **TT** units are further anchored to each other by several short C-H...N HBs in the plane roughly perpendicular to the stacking axis. On the other hand, the pyridinic ring, slightly rotated with respect to the **TT** plane, is involved only in weak interactions resulting in conformational freedom which is at the basis of the formation of the three polymorphs.

Extensive spectroscopical, structural and theoretical investigation on **TT-2Py** evidenced the presence of both molecular and supramolecular radiative deactivation channels in its complex solid-state photophysical behavior (see Table 1 and Fig. 1). In particular,  $\pi$ - $\pi$  interactions among **TT** units were deemed responsible for low energy phosphorescence (LEP), while the remaining emissions, namely HEF (high energy fluorescence), HEP (high energy phosphorescence), MEP (medium energy phosphorescence) and LEF (low energy fluorescence), were associated with molecular electronic states.

**Table 1.** Photophysical parameters of crystals of **TT-2Py** (polymorph A), blended **TT-2Py**/PMMA (w/w 10 %) films and crystals of (**TT-2PyH<sup>+</sup>**NO<sub>3</sub>)·H<sub>2</sub>O.

298 K				
	$\Phi$	$\lambda_{em}$ (nm)	$\tau$	Origin
<b>TT-2Py</b> (polymorph A)	52	370	698 ms	HEP
		418	0.29 ms	MEP
		450		LEF
		510, 570, 608	2.09 ms	LEP
<b>TT-2Py</b> /PMMA		350	1.18 ns	HEF
		394	13.73 ms	MEP
		440	3.47 ns	LEF
		530	15.70ms	LEP
<b>(TT-2PyH<sup>+</sup></b> NO <sub>3</sub> )·H <sub>2</sub> O	12	412	1.90 ns	HEF
		482	4.66 ms	MEP
		548	131.11 ms	LEP

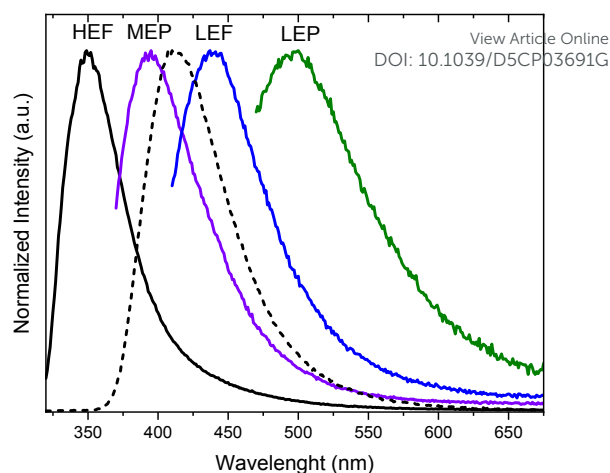


**Fig. 1** Photophysical properties of **TT-2Py** in PMMA (**TT-2Py**/PMMA 10% wt) before (solid lines) and after (dashed line) HCl exposure. Emission spectra  $\lambda_{exc}$  = 300 nm (black lines),  $\lambda_{exc}$  = 350 nm (violet),  $\lambda_{exc}$  = 390 nm (blue), and  $\lambda_{exc}$  = 450 nm (green).

Specifically, DFT calculations on **TT-2Py** revealed the presence of two almost isoenergetic minima (A and C, Fig. 2, left panel) in the  $S_0$  potential energy surface of the molecule, separated by a very small energy barrier (B, ~2 kcal/mol). The more stable A conformation, with the pyridinic nitrogen atom pointing on the opposite site with respect to the **TT** one, corresponds to the X-ray structure observed in all the three polymorphs, while in C the two nitrogen atoms face each other. Consequently, HEF (clearly visible only in PMMA film being overlapped with HEP in crystals) was associated (see Fig. 2, left panel) with radiative deactivation from the first singlet excited state ( $S_1$ ) of molecules in A conformation (representing the majority). HEP was explained as an anti-Kasha emission from a high energy triplet state ( $T_n$ ) of ( $\sigma/\pi, \pi^*$ ) character with slow internal conversion (IC) to the ( $\pi, \pi^*$ )  $T_1$  one, from which MEP is originated. Finally, LEF was attributed to the fraction of molecules in the C minimum through excitation to a triplet  $T_m$  of low energy, followed by ISC to  $S_1$ . Though conformer C was not observed in any of the **TT-2Py** polymorphs, its minority presence cannot be excluded in blended films and, as defect, in the crystal phase due to the low energy barrier from minimum A. This rather complex mechanism was also supported by pump-probe experiments.

Here, to further strength the hypothesis that conformational freedom is responsible for the appearance of dual fluorescence of **TT-2Py**, we have prepared and characterized its derivative with protonated pyridinic nitrogen, **TT-2PyH<sup>+</sup>**, considering that H-bonds could lock the molecular geometry.



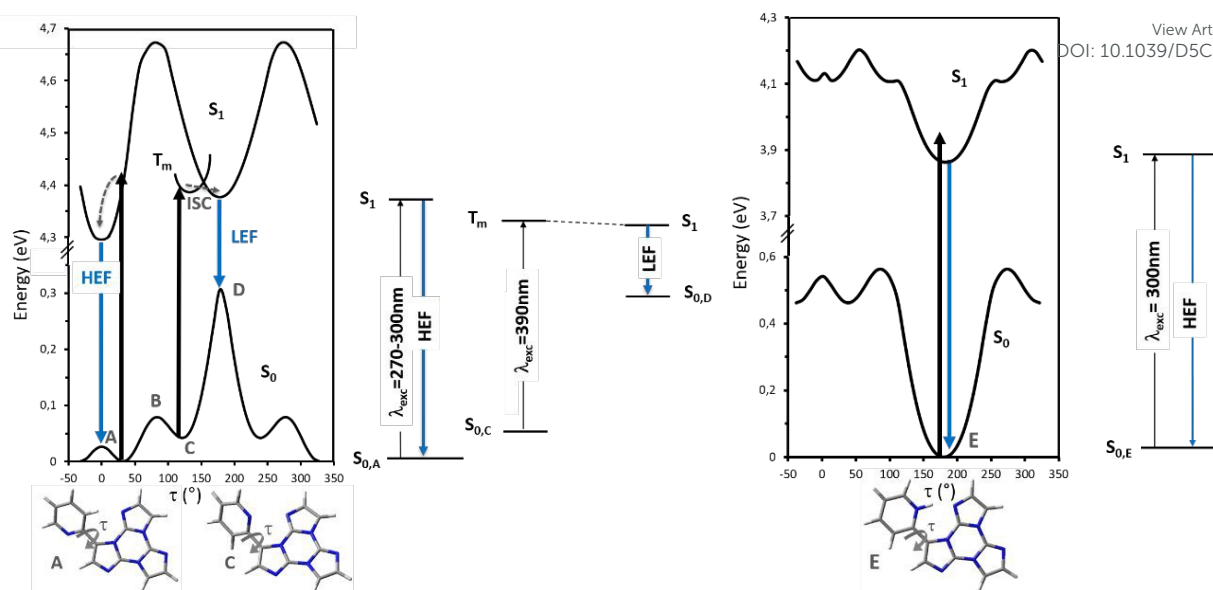


**Fig. 2** Scans of the relaxed potential energy surfaces of  $S_1$  and  $S_0$  and simplified Jablonski diagrams for fluorescent emissions of **TT-2Py** (left) and **TT-2PyH<sup>+</sup>** (right) along the  $N_{py}-C_{py}-C_{TT}-C_{TT}$  torsion angle,  $\tau$ , at the (TD)- $\omega$ B97X/6-311++G(d,p) level of theory.  $T_m$  represents a generic triplet level, A, C and E denote minima on  $S_0$  of **TT-2Py** and **TT-2PyH<sup>+</sup>** and B is the barrier between the two minima on  $S_0$  of **TT-2Py**. Energies are relative to the  $S_0$  state equilibrium geometry.

**TT-2PyH<sup>+</sup>NO<sub>3</sub><sup>-</sup>** was synthesized by reaction of **TT-2Py** with HNO<sub>3</sub> in DCM/MeOH (see the Experimental) and characterized by single crystal X-ray diffraction and multinuclear <sup>1</sup>H, <sup>13</sup>C and <sup>15</sup>N NMR spectroscopy in DMSO-*d*<sub>6</sub> solution (see Fig. S12-S17). A comparison with <sup>1</sup>H NMR of **TT-2Py** shows that after protonation all signals display a downfield shift ( $\Delta\delta \sim 0.1 - 0.5$  ppm) with the largest values for the H atoms of the pyridine ring and for the singlet of the imidazole core (see Fig. 3). A similar effect was observed after complexation of **TT-2Py** to rhenium(I) carbonyl derivatives.<sup>31</sup> In addition, a triplet at 7.11 ppm characteristic for a NH<sup>+</sup> signal with  $J$  of 51.1 Hz due to <sup>14</sup>N-<sup>1</sup>H coupling appears in the spectrum,<sup>36</sup> confirming that the structure is retained in DMSO-*d*<sub>6</sub> solution even though the integral value of the latter signal is slightly lower than the expected value probably due to some exchange with deuterium.

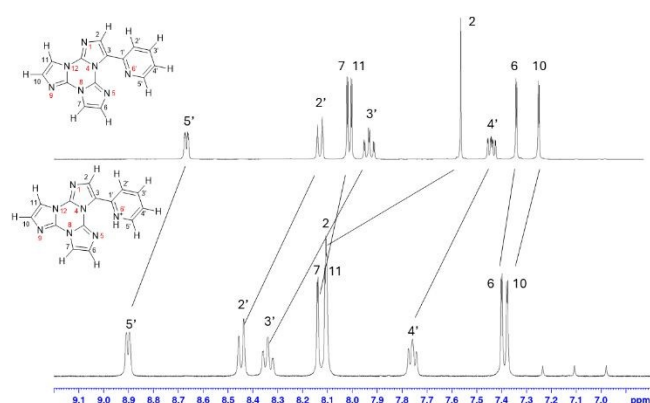


**Fig. 3** <sup>1</sup>H-NMR spectra of **TT-2Py** (upper trace) and **TT-2PyH<sup>+</sup>NO<sub>3</sub><sup>-</sup>** (lower trace) (298 K, DMSO-*d*<sub>6</sub>, 400 MHz).

<sup>15</sup>N NMR spectroscopy performed by carrying out 2D <sup>1</sup>H-<sup>15</sup>N heteronuclear long-range correlation (HMBC) experiments (Fig.

S16 and S17) shows chemical shifts in the 150 and 220 ppm regions, respectively assigned to the triazine-based core and the imidazole rings on the basis of previous studies<sup>37</sup> together with a signal at 18 ppm due to the protonated pyridine nitrogen, while no signals in the 310 ppm region typical for the nitrogen resonance of pyridine have been detected.<sup>38</sup>

Single crystal X-ray diffraction studies performed at 150 and 299 K revealed that the compound crystallizes in the P-1 space group including, in its asymmetric unit, a water molecule (Fig. 4 and Table S1). In the (**TT-2PyH<sup>+</sup>NO<sub>3</sub><sup>-</sup>**)·H<sub>2</sub>O crystal structure, the NO<sub>3</sub><sup>-</sup> anion is hydrogen bonded (HB) to both imidazolic and pyridinic hydrogen atoms and the water molecule which, in turn, acts as HB acceptor from a pyridinic hydrogen atom. The main difference between the 150 and 299 K structures is the presence of a minor disordered component of NO<sub>3</sub><sup>-</sup> in the latter. **TT-2PyH<sup>+</sup>** adopts a virtually planar and locked conformation thanks to the formation of a strong N-H<sup>+</sup>...N intramolecular HB ( $r_{H...N} = 1.85$  Å) bridging the protonated pyridinic nitrogen atom with the closest nitrogen of **TT**, generating a 7-membered cyclic structure. Thus, hydrogen bond is the driving force to massively rotate, by almost 180°, the pyridinic moiety with respect to the orientation assumed in **TT-2Py** (A minimum in Fig. 2, left panel). This locked structure was previously predicted by DFT scan calculations on the **TT-2PyH<sup>+</sup>**  $S_0$  PES (Fig. 2, right panel),<sup>28</sup> evidencing the great stabilization accompanying such rotation during the protonation process, leading to a single, deep well (E).

The chromophores are organized into infinite zig-zag ribbons through relatively strong centrosymmetric C-H...N HBs ( $r_{H...N} = 2.33$  and 2.37 Å, see Fig. 4, top). Ribbons are laterally connected to each other through bridging NO<sub>3</sub><sup>-</sup> counterions, lying almost in the same plane of the ribbons. As a result, infinite extended plates are formed, where the two ions, together with water which fills the spaces within ribbons, interdigitate forming a





dense HB network ( $r_{\text{C(H)}\cdots\text{O(N)}}$  in the 2.33–2.60 Å range,  $r_{\text{C(H)}\cdots\text{O(H)}} = 2.45, 2.60$  Å and  $r_{\text{O(H)}\cdots\text{O(N)}} = 1.92, 1.99$  Å, parameters, here and below, referring to the structure determined at 150 K, see Table S2). The layers stack in quite largely slipped head-to-tail arrangement of the **TT** units (see Fig. 4, bottom), with alternating separations between the layers of 3.074 and 3.202 Å and corresponding distances between triazinic geometrical centroids of 5.494 and 5.188 Å. Cations from adjacent layers overlap the imidazolic subunits opposite to pyridine, with shortest contacts  $r_{\text{C6}\cdots\text{C7}(1-x,1-y,1-z)} = 3.200(2)$  Å,  $r_{\text{C6}\cdots\text{N5}(1-x,1-y,1-z)} = 3.228(2)$  Å, from one side, and  $r_{\text{C9}\cdots\text{C7}(1-x,2-y,1-z)} = 3.249(2)$  Å from the other side of the reference molecule. Additional short contacts with the H-bonded centrosymmetry-related equivalent ( $r_{\text{C1}\cdots\text{C4}(1+x,y,z)} = 3.327(2)$  Å and  $r_{\text{C9}\cdots\text{C5}(1+x,y,z)} = 3.389(2)$  Å) are found from both sides of the molecule. Such multiple short C $\cdots$ C and C $\cdots$ N distances along the crystallographic *b* axis denote the presence of columnar aggregates associated with the establishment of strong  $\pi$ - $\pi$  stacking interactions among the chromophores, despite the large molecules' slippage. Quite similar stacking features have been found in polymorph A of the parent **TT-2Py** neutral derivative, displaying several C $\cdots$ C close contacts with comparable distance (5.358 Å) between triazinic centroids. The anions are placed, along *b*, approximately halfway between two pyridinic rings, with closest cation–anion centroids distance ( $r_{\text{C}\cdots\text{A}}$ ) equal to 3.829 Å.

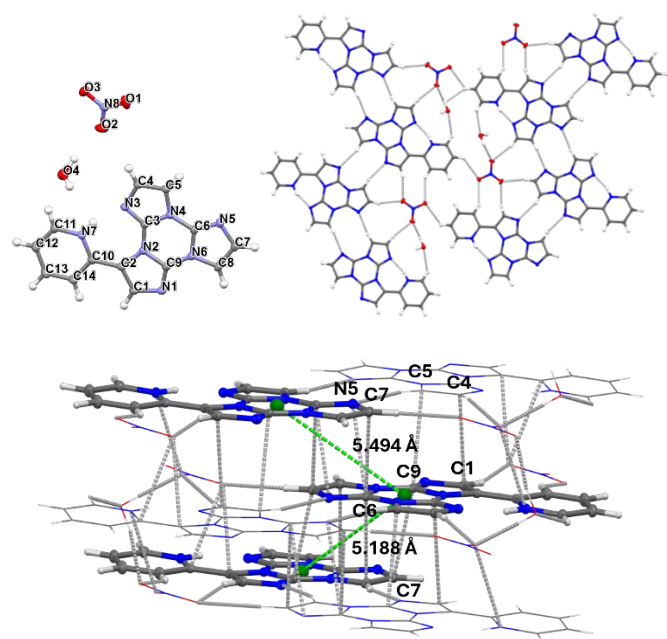


**Fig. 4** Crystal structure of **(TT-2PyH<sup>+</sup>NO<sub>3</sub><sup>-</sup>)·H<sub>2</sub>O** at 150 K: asymmetric unit (top left) and packing fragments showing the HB network (top right) and the  $\pi$ - $\pi$  stacking motif highlighting the head-to-tail arrangement of the chromophores (bottom). Intermolecular contacts below the sum of vdW radii (dashed grey lines) and selected triazinic geometrical centroids (green spheres) are included. Ellipsoids at 20% probability.

Intermolecular geometric parameters respond to temperature variation in quite different way. Going from 150 to 299 K,  $r_{\text{C}\cdots\text{A}}$  undergoes a large increase (0.1 Å) to 3.925 Å; the shortest C $\cdots$ C/N contacts display a usual 0.04–0.05 Å increase ( $r_{\text{C6}\cdots\text{C7}(1-x,1-y,1-z)} = 3.252(3)$  Å,  $r_{\text{C9}\cdots\text{C7}(1-x,2-y,1-z)} = 3.287(3)$  Å); and, notably, H-

bonds linking the chromophores are virtually independent on temperature (see Table S2), indicating rigid interchromophoric connection through HB.<sup>39–43</sup>

To visualize and quantify the different intermolecular interactions governing the structure of the **(TT-2PyH<sup>+</sup>NO<sub>3</sub><sup>-</sup>)·H<sub>2</sub>O**, a Hirshfeld surface analysis (HSA)<sup>44</sup> has been performed. Particularly illuminating for the present structure are plots of HSs mapped with  $d_{\text{norm}}$ , curvedness (*C*) and shape index (*S*), where  $d_{\text{norm}}$  is the sum of normalised (with vdW radii)  $d_i$  and  $d_e$ , the distances from the Hirshfeld surface to the nearest nucleus inside and outside the surface, respectively. *C* and *S* are both defined in terms of the HS principal curvatures, the former depending on the root-mean-square curvature of the surface, and the latter providing a qualitative description of its shape, identifying complementary hollows (red) and bumps (blue regions), associated respectively to acceptor and donor entities of the interaction<sup>45</sup> Fig. 5 shows HSs mapped with  $d_{\text{norm}}$ , *C* and *S* for **TT-2PyH<sup>+</sup>** within the crystal, including for clarity the counterion, a water molecule and other protonated species interacting with the reference one along the stacking axis. The map with  $d_{\text{norm}}$  (Fig. 5, left) clearly indicates strength and type of intermolecular interactions, with red regions (i.e. with distances shorter than the sum of vdW radii) being found in proximity of nitrogen and hydrogen atoms or over carbon atoms, and therefore attributable, respectively, to hydrogen bonds or  $\pi$ - $\pi$  stacking interactions involving these atoms. The curvedness map (Fig. 5, center), characterized by extended green regions (i.e. having low curvature) separated by blue edges (large curvatures) gives evidence of the planar stacking between molecules. The patterns of red-orange spots on the shape index surface (Fig. 5, right) are diagnostic for close C $\cdots$ C/N interplanar contacts, denoting the areas involved in  $\pi$ - $\pi$  stacking interaction.<sup>46</sup>

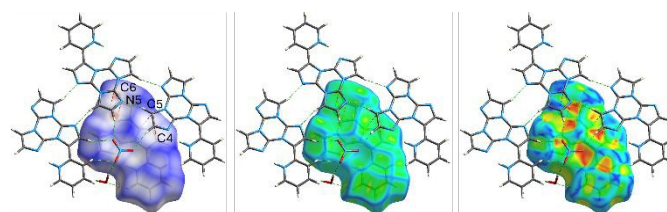


**Fig. 5** Hirshfeld surface for **TT-2PyH<sup>+</sup>** mapped with  $d_{\text{norm}}$  (left), curvedness (center) and shape index (right) with X $\cdots$ Y contacts and hydrogen bonds (red and green dashed lines, respectively) shorter than the sum of the vdW radii.

When excited at high energy (300–370 nm), crystals of **(TT-2PyH<sup>+</sup>NO<sub>3</sub><sup>-</sup>)·H<sub>2</sub>O** display at room temperature a multicomponent broad emission (Fig. 6 and Table 1) comprising one fluorescence (at 412 nm,  $\tau = 1.90$  ns, Fig. S2) as a shoulder of a much stronger phosphorescence (at 482 nm,  $\tau = 4.66$  ms; overall  $\Phi = 12\%$ , Fig. S3), with this latter isolated by exciting at sufficiently low energy to exclude the high energy peak ( $\lambda_{\text{exc}} \sim 412$  nm). By exciting at 480 nm an additional long-lived emission (at 548 nm,  $\tau = 131.11$  ms, Fig. S4), which is overwhelmed by the stronger high energy components at high energy excitations, appears in the spectrum. These spectral features, which are maintained at 77 K, can be considered as the red-shifted analogue of the neutral molecule HEF, MEP and LEP. The



prolonging of lifetimes at low temperature (3.23 ns, 24.27 ms and 550 ms, respectively, Fig. S6-S8) indicates inhibition of thermal quenching especially for the long-lived components ( $\tau_{77K} / \tau_{298K} = 1.7$  for HEF, 5.2 for MEP and 4.2 for LEP). The presence of only one minimum in both the **TT-2PyH<sup>+</sup>**  $S_0$  and  $S_1$  PESs (Fig. 2, right panel) explains the observation of only one fluorescence (HEF) in crystals of **(TT-2PyH<sup>+</sup>NO<sub>3</sub>)·H<sub>2</sub>O**. At the same time, the absence of LEF, resulting from locking the molecules in a rigid conformation through intramolecular HB, confirms molecular flexibility at its origin in **TT-2Py**. Moreover, in agreement with previously reported TDDFT calculations,<sup>28</sup> anti-Kasha HEP is not observed for **TT-2PyH<sup>+</sup>** having only ( $\pi, \pi^*$ ) levels (see Fig. S11 for a full picture of the **TT-2Py** and **TT-2PyH<sup>+</sup>** electronic levels including Natural Transition Orbitals for selected transitions). The only observed molecular phosphorescence, MEP, is explained as radiative deactivation from  $T_1$  reached, after IC, through easy ISC from  $S_1$  to the almost overlapped  $T_4$  level. These results also agree with what previously observed for **TT-2Py** blended PMMA films exposed to acidic vapors to give **TT-2PyH<sup>+</sup>** which showed a single fluorescence (at 412 nm, Fig. 1), together with a weak phosphorescence, both at lower energy with respect to the corresponding ones of **TT-2Py**.

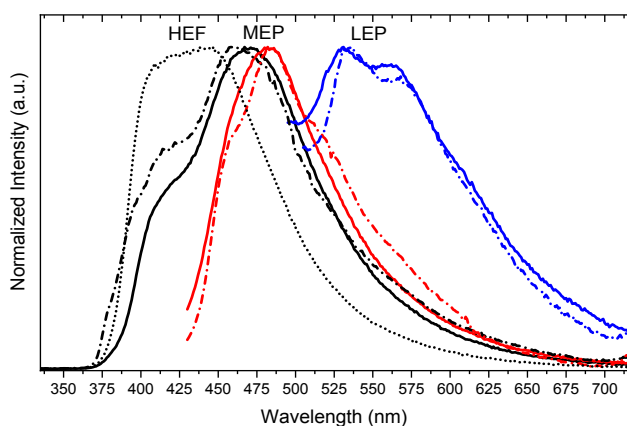


**Fig. 6** Emission spectra of **(TT-2PyH<sup>+</sup>NO<sub>3</sub>)·H<sub>2</sub>O** crystals at 298 K (full lines) and 77 K (dashed dotted lines).  $\lambda_{exc}$ : 300 nm (black lines), 412 nm (red lines) and 480 nm (blue lines). Emission spectrum of crystals after grinding at 298 K and 300 nm excitation is also reported (black dotted line).

Compared with previous results on **TT-2PyH<sup>+</sup>**/PMMA, the strong intensification of MEP relative to HEF in **TT-2PyH<sup>+</sup>** crystals can be interpreted as due to rigidification and protection from oxygen quenching through intermolecular interactions resulting in crystallization induced features. Moreover, previous investigation on the effects of ion-pairing on the emissive properties of benzimidazolium salts demonstrated that a close cation–anion centroids distance, as observed in the present compound, favors molecular phosphorescence at the expense of the corresponding fluorescence.<sup>47</sup> A crystalline induced effect is supported by measurements on ground **TT-2PyH<sup>+</sup>** crystals which display a slight increase of the overall quantum efficiency (14.5%) accompanied by a reduction of MEP intensity relative to HEF (Fig. S9) suggesting an easier singlet-triplet ISC process in crystalline **TT-2PyH<sup>+</sup>**.

## Materials and Methods

All reagents and model molecules were purchased from chemical suppliers and used without further purification unless otherwise stated. **TT-2Py** was prepared according to literature procedures.<sup>28</sup>

<sup>1</sup>H, <sup>13</sup>C and <sup>15</sup>N NMR spectra were recorded on a Bruker AVANCE-400 instrument (400 MHz). Chemical shifts are reported in parts per million (ppm) and are referenced to the residual solvent peak (DMSO, <sup>1</sup>H 2.50 ppm, <sup>13</sup>C 39.50 ppm) and to NH<sub>3</sub> for <sup>15</sup>N resonances. Coupling constants (*J*) are given in hertz (Hz) and are quoted to the nearest 0.5 Hz. Peak multiplicities are described in the following way: s, singlet; d, doublet; t, triplet; m, multiplet.

## Synthesis of **TT-2PyH<sup>+</sup>NO<sub>3</sub><sup>-</sup>**

**TT-2Py** (0.035 g, 0.127 mmol) was dissolved at room temperature in a 2:1 DCM(10mL)/MeOH(5mL) mixture inside a 25 mL round bottom flask equipped with a magnetic stirrer. Two drops of concentrated nitric acid were added to the mixture that was kept under stirring for 1h at room temperature. Single crystals of **(TT-2PyH<sup>+</sup>NO<sub>3</sub><sup>-</sup>)·H<sub>2</sub>O** suitable for XRD analysis were obtained in few days by slow evaporation of the solvent mixture.

NMR data for **TT-2PyH<sup>+</sup>NO<sub>3</sub><sup>-</sup>** (9.4 T, DMSO-*d*<sub>6</sub>, 298 K,  $\delta$ , ppm): <sup>1</sup>H NMR 8.90 (d, *J* = 5.1, 1H), 8.44 (d, *J* = 8.1 Hz, 1H), 8.33 (m, 1H), 8.13 (d, *J* = 1.5 Hz, 1H), 8.10 (d, *J* = 1.5 Hz, 1H), 8.08 (s, 1H), 7.75 (m, 1H), 7.39 (d, *J* = 1.5 Hz, 1H), 7.37 (d, *J* = 1.5 Hz, 1H), 7.11 (t, *J* = 51.1 Hz, 1H). <sup>13</sup>C NMR: 144.89 (CH), 143.67 (C), 141.39 (CH), 138.28 (C), 136.00 (C), 135.47 (C), 133.05 (CH), 129.10 (CH), 127.18 (CH), 125.07 (CH), 124.18 (CH), 123.50 (C), 112.27 (CH), 112.09 (CH). <sup>15</sup>N NMR: 220.9, 219.0, 154.6, 150.2, 18.6 (Fig. S12-S17).

## X-ray diffraction studies.

X-ray data of **(TT-2PyH<sup>+</sup>NO<sub>3</sub><sup>-</sup>)·H<sub>2</sub>O** have been collected at 150 and 299 K on a Rigaku XtaLAB Synergy S X-ray diffractometer (Rigaku Co., Tokyo, Japan) operated with a mirror-monochromated micro-focus Cu-K $\alpha$  radiation ( $\lambda$  = 1.54184 Å) at 50 kV and 1.0 mA and equipped with a CCD HyPix 6000 detector. The structure has been solved using direct methods and refined with SHELXL-19<sup>48</sup> using a full-matrix least squares procedure based on F<sup>2</sup> using all data. Hydrogen atoms have been placed at geometrically estimated positions. Details relating to the crystal and the structural refinement are presented in Table S1. Full details of crystal data and structure refinement, in CIF format, are available as Supplementary Information. Hydrogen atoms were placed at geometrically estimated positions except those of the water co-crystallized molecule. Their position was refined by fixing the O–H and H...H distances with DFIX and DANG restraints, respectively. Crystal data and results of structural refinement are summarized in Table S1, while full details, in CIF format, are available as Supplementary Information. CCDC reference numbers: 2401405 and 2401406 for the structures collected at 150 and 299 K, respectively.



**Computational details.**

DFT and TDDFT calculations on isolated 'gas-phase' **TT-2PyH<sup>+</sup>** ion were performed with Gaussian 16 program (Revision A.03)<sup>49</sup> using the 6-311++G(d,p) basis set. Geometry optimization has been carried out starting from the corresponding X-ray molecular structure. The  $\omega$ B97X<sup>50</sup> functional was adopted throughout, owing to its good performance in describing not only ground and excited states properties (though slightly overestimating excitation electronic energies), but also intermolecular interactions including in particular  $\pi$ - $\pi$  interactions. Further details are reported as Supporting Information.

**Photophysical characterization**

Photoluminescence quantum yields have been measured using a C11347 Quantaaurus–Absolute Photoluminescence Quantum Yield Spectrometer (Hamamatsu Photonics K.K), equipped with a 150 W Xenon lamp, an integrating sphere and a multichannel detector. Steady state emission and excitation spectra and photoluminescence lifetimes have been obtained using a FLS 980 (Edinburg Instrument Ltd) spectrofluorimeter. The steady state measurements have been recorded by a 450 W Xenon arc lamp. Photoluminescence lifetime measurements have been performed using a EPLED-300 (Edinburg Instrument Ltd) and microsecond flash Xe-lamp (60W, 0.1÷100 Hz) with data acquisition devices time correlated single-photon counting (TCSPC) and multi-channel scaling (MCS) methods, respectively. Average lifetimes are obtained as  $\tau_{av} = \frac{\sum A_i \tau_i^2}{\sum A_i \tau_i}$  from bi-exponential or three-exponential fits. Low temperature measurements have been performed by immersion of the sample in a liquid N<sub>2</sub> quartz dewar.

**Conclusions**

Intra- and intermolecular interactions play a key role in materials' photophysical behavior. Besides their proven ability to reduce competitive non-radiative deactivation channels, more subtle effects do exist and still need deeper investigation. In the present article, the effects of HB and  $\pi$ - $\pi$  stacking interactions on the emissive features of **TT-2Py** and **TT-2PyH<sup>+</sup>** are disclosed. While  $\pi$ - $\pi$  interactions activate ultralong phosphorescence in both compounds, intramolecular HB in **TT-2PyH<sup>+</sup>** is demonstrated to suppress, through conformational locking, the low energy fluorescence of **TT-2Py** as originally proposed. This work therefore provides a further contribution in understanding the relationship between molecular structures and photoluminescence performance at the molecular and aggregate levels.

**Author contributions**

Conceptualization, D. Mal., E. L., E. C. and A. F.; methodology, D. Mal., E. L., E. C. and A. F.; investigation, all authors; supervision, E. C. and A. F.; writing—original draft preparation: E. C. and A. F.; writing—review and editing: all authors.

**Conflicts of interest**

There are no conflicts to declare.

**Data availability**

The data supporting this article have been included as part of the Supplementary Information.

**Acknowledgements**

D.M. acknowledges Fondazione Cariplo for financial support (Giovani Ricercatori, 2024-0439). The use of instrumentation purchased through the Regione Lombardia – Fondazione Cariplo joint SmartMatLab Project is gratefully acknowledged. XRD data have been collected at the SCXRD facility of the Unitech COSPECT at the University of Milan (Italy).

**Notes and references**

- Q. Dang, Y. Jiang, J. Wang, J. Wang, Q. Zhang, M. Zhang, S. Luo, Y. Xie, K. Pu, Q. Li and Z. Li, *Adv. Mater.*, 2020, **32**, 2006752.
- W. Qin, P. Zhang, H. Li, J. W. Y. Lam, Y. Cai, R. T. K. Kwok, J. Qian, W. Zheng and B. Z. Tang, *Chem. Sci.*, 2018, **9**, 2705.
- Y. Wang, H. Gao, J. Yang, M. Fang, D. Ding, B. Z. Tang and Z. Li, *Adv. Mater.*, 2021, **33**, 2007811.
- L. Gu, H. Wu, H. Ma, W. Ye, W. Jia, H. Wang, H. Chen, N. Zhang, D. Wang, C. Qian, Z. An, W. Huang and Y. Zhao, *Nat. Commun.*, 2020, **11**, 944.
- Y. Lei, W. Dai, J. Guan, S. Guo, F. Ren, Y. Zhou, J. Shi, B. Tong, Z. Cai, J. Zheng and Y. Dong, *Angew. Chem. Int. Ed.*, 2020, **59**, 16054.
- Y. Li and P. Gao, *Chemosensors*, 2023, **11**, 489.
- B. Sk and S. Hirata, *Adv. Sci.*, 2024, **11**, 2308897.
- J. Tan, Q. Li, S. Meng, Y. Li, J. Yang, Y. Ye, Z. Tang, S. Qu and X. Ren, *Adv. Mater.*, 2021, **33**, 2006781.
- S. Hirata, K. Totani, H. Kaji, M. Vacha, T. Watanabe and C. Adachi, *Adv. Opt. Mater.*, 2013, **1**, 438.
- X. Ma, J. Wang and H. Tian, *Acc. Chem. Res.*, 2019, **52**, 738.
- X.-K. Ma and Y. Liu, *Acc. Chem. Res.*, 2021, **54**, 3403.
- H. Shi, W. Yao, W. Ye, H. Ma, W. Huang and Z. An, *Acc. Chem. Res.*, 2022, **55**, 3445.
- X. Yang, G. I. N. Waterhouse, S. Lu and J. Yu, *Chem. Soc. Rev.*, 2023, **52**, 8005.
- W. Zhao, Z. He and B. Z. Tang, *Nat. Rev. Mater.*, 2020, **5**, 869.
- S. Cai, H. Shi, J. Li, L. Gu, Y. Ni, Z. Cheng, S. Wang, W.-w. Xiong, L. Li, Z. An and W. Huang, *Adv. Mater.*, 2017, **29**, 1701244.
- S. Cai, X. Yao, H. Ma, H. Shi and Z. An, *Aggregate*, 2023, **4**, e320.
- C. Demangeat, M. Remond, T. Roisnel, C. Quinton and L. Favereau, *Chem. Eur. J.*, 2024, **30**, e202401506.
- L. Gu, H. Shi, M. Gu, K. Ling, H. Ma, S. Cai, L. Song, C. Ma, H. Li, G. Xing, X. Hang, J. Li, Y. Gao, W. Yao, Z. Shuai, Z. An, X. Liu and W. Huang, *Angew. Chem. Int. Ed.*, 2018, **57**, 8425.
- A. Jamadar, A. K. Singh, L. Roy and A. Das, *J. Mater. Chem. C*, 2021, **9**, 11893.



- 20 X.-N. Li, M. Yang, X.-L. Chen, J.-H. Jia, W.-W. Zhao, X.-Y. Wu, S.-S. Wang, L. Meng and C.-Z. Lu, *Small*, 2019, **15**, 1903270.
- 21 E. Lucenti, A. Forni, C. Botta, L. Carlucci, C. Giannini, D. Marinotto, A. Previtali, S. Righetto and E. Cariati, *J. Phys. Chem. Lett.*, 2017, **8**, 1894.
- 22 S. Sujilkumar, A. Kalyani and M. Hariharan, *Chem. Commun.*, 2025, **61**, 5463.
- 23 J. Zhou, L. Stojanović, A. A. Berezin, T. Battisti, A. Gill, B. M. Kariuki, D. Bonifazi, R. Crespo-Otero, M. R. Wasielewski and Y.-L. Wu, *Chem. Sci.*, 2021, **12**, 767.
- 24 Z. Chai, C. Wang, J. Wang, F. Liu, Y. Xie, Y.-Z. Zhang, J.-R. Li, Q. Li and Z. Li, *Chem. Sci.*, 2017, **8**, 8336.
- 25 M. Fang, J. Yang, X. Xiang, Y. Xie, Y. Dong, Q. Peng, Q. Li and Z. Li, *Mater. Chem. Front.*, 2018, **2**, 2124.
- 26 H. Li, J. Gu, Z. Wang, J. Wang, F. He, P. Li, Y. Tao, H. Li, G. Xie, W. Huang, C. Zheng and R. Chen, *Nat. Commun.*, 2022, **13**, 429.
- 27 A. Forni, D. Malpicci, D. Maver, E. Lucenti and E. Cariati, *J. Mater. Chem. C*, 2025, **13**, 3721.
- 28 E. Lucenti, A. Forni, A. Previtali, D. Marinotto, D. Malpicci, S. Righetto, C. Giannini, T. Virgili, P. Kabacinski, L. Ganzer, U. Giovanella, C. Botta and E. Cariati, *Chem. Sci.*, 2020, **11**, 7599.
- 29 D. Malpicci, S. R. Araneo, S. Arnaboldi, E. Cariati, A. Forni, S. Grecchi, E. Lucenti, D. Marinotto, D. Maver and P. R. Mussini, *Electrochim. Acta*, 2023, **469**, 143117.
- 30 D. Malpicci, D. Blasi, D. Marinotto, A. Forni, E. Cariati, E. Lucenti and L. Carlucci, *Crystals*, 2023, **13**, 149.
- 31 D. Malpicci, D. Maver, D. Maggioni, P. Mercandelli, L. Carlucci, E. Cariati, P. Mussini and M. Panigati, *New J. Chem.*, 2023, **47**, 21463.
- 32 E. Melnic, V. C. Kravtsov, E. Lucenti, E. Cariati, A. Forni, N. Siminel and M. S. Fonari, *New J. Chem.*, 2021, **45**, 9040.
- 33 M. S. Fonari, V. C. Kravtsov, V. Bold, E. Lucenti, E. Cariati, D. Marinotto and A. Forni, *Cryst. Growth Des.*, 2021, **21**, 4184.
- 34 E. Lucenti, E. Cariati, A. Previtali, D. Marinotto, A. Forni, V. Bold, V. C. Kravtsov, M. S. Fonari, S. Galli and L. Carlucci, *Cryst. Growth Des.*, 2019, **19**, 1567.
- 35 D. Malpicci, E. Lucenti, A. Forni, D. Marinotto, A. Previtali, L. Carlucci, P. Mercandelli, C. Botta, S. Righetto and E. Cariati, *Inorg. Chem. Front.*, 2021, **8**, 1312.
- 36 T. D. W. Claridge, in *High-Resolution NMR Techniques in Organic Chemistry (Third Edition)*, ed. T. D. W. Claridge, Elsevier, Boston, 2016, DOI: <https://doi.org/10.1016/B978-0-08-099986-9.00007-5>, pp. 243.
- 37 S. Di Micco, C. Giannini, A. Previtali, E. Lucenti and G. Bifulco, *Magn. Reson. Chem.*, 2019, **57**, 82.
- 38 P. Beltrame, E. Cadoni, C. Floris, G. Gelli and A. Lai, *Spectrochim. Acta, Part A*, 2002, **58**, 2693.
- 39 S. Bhattacharya and B. K. Saha, *Cryst. Growth Des.*, 2013, **13**, 3299.
- 40 A. Forni, P. Metrangolo, T. Pilati and G. Resnati, *Cryst. Growth Des.*, 2004, **4**, 291.
- 41 V. G. Saraswatula and B. K. Saha, *New J. Chem.*, 2014, **38**, 897.
- 42 V. G. Saraswatula and B. K. Saha, *Chem. Commun.*, 2015, **51**, 9829.
- 43 V. G. Saraswatula, D. Sharada and B. K. Saha, *Cryst. Growth Des.*, 2018, **18**, 52.
- 44 P. R. Spackman, M. J. Turner, J. J. McKinnon, S. K. Wolff, D. J. Grimwood, D. Jayatilaka and M. A. Spackman, *J. Appl. Crystallogr.*, 2021, **54**, 1006.
- M. A. Spackman and D. Jayatilaka, *CrystEngComm*, 2009, **11**, 19. DOI: 10.1039/D5CP03691G
- J. J. McKinnon, M. A. Spackman and A. S. Mitchell, *Acta Cryst. Sect. B*, 2004, **60**, 627.
- G. Di Carlo, A. Forni, P. Moretti, D. Marinotto, C. Botta, M. Pizzotti, F. Tessore and E. Cariati, *J. Mater. Chem. C*, 2021, **9**, 4182.
- G. M. Sheldrick, *Acta Crystallogr. C Struct. Chem.*, 2015, **71**, 3.
- M. J. Frisch, G. W. Trucks, H. B. Schlegel, G. E. Scuseria, M. A. Robb, J. R. Cheeseman, G. Scalmani, V. Barone, G. A. Petersson, H. Nakatsuji, X. Li, M. Caricato, A. V. Marenich, J. Bloino, B. G. Janesko, R. Gomperts, B. Mennucci, H. P. Hratchian, J. V. Ortiz, A. F. Izmaylov, J. L. Sonnenberg, Williams, F. Ding, F. Lipparini, F. Egidi, J. Goings, B. Peng, A. Petrone, T. Henderson, D. Ranasinghe, V. G. Zakrzewski, J. Gao, N. Rega, G. Zheng, W. Liang, M. Hada, M. Ehara, K. Toyota, R. Fukuda, J. Hasegawa, M. Ishida, T. Nakajima, Y. Honda, O. Kitao, H. Nakai, T. Vreven, K. Throssell, J. A. Montgomery Jr., J. E. Peralta, F. Ogliaro, M. J. Bearpark, J. J. Heyd, E. N. Brothers, K. N. Kudin, V. N. Staroverov, T. A. Keith, R. Kobayashi, J. Normand, K. Raghavachari, A. P. Rendell, J. C. Burant, S. S. Iyengar, J. Tomasi, M. Cossi, J. M. Millam, M. Klene, C. Adamo, R. Cammi, J. W. Ochterski, R. L. Martin, K. Morokuma, O. Farkas, J. B. Foresman and D. J. Fox, *Gaussian 16 Rev. A.03*, Wallingford, CT, 2016.
- J.-D. Chai and M. Head-Gordon, *J. Chem. Phys.*, 2008, **128**, 084106.





View Article Online  
DOI: 10.1039/D5CP03691G

## Data availability statement

The data supporting this article have been included as part of the Supplementary Information.

